22. Jahren, A. H., Arens, N. C., Sarmiento, G., Guerro, J. & Amundson, R. Terrestrial record of methane hydrate dissociation in the Early Cretaceous. *Geology* **29,** 159–162 (2001).
23. Arens, N. C. & Jahren, A. H. Carbon isotope excursion in atmospheric CO_2 at the Cretaceous-Tertiary boundary: evidence from terrestrial sediments. *Palaios* **15,** 314–322 (2000).
24. Khalil, M. A. K. (ed.) *Atmospheric Methane* 86 (Springer, Berlin, 2000).
25. McGowran, B. & Li, Q.-Y. Miocene climatic oscillation recorded in the Lakes Entrance oil shaft, southern Australia. *Aust. J. Earth Sci.* **43,** 129–148 (1997).
26. Utescher, T., Mossbrugger, U. & Ashraf, A. R. Terrestrial climate evolution in northwest Germany over the last 25 million years. *Palaios* **15,** 430–449 (2000).
27. Schwartz, T. Lateritic bauxite in central Germany and implications for Miocene palaeoclimates. *Palaeogeogr. Palaeoclimatol. Palaeoecol.* **129,** 37–50 (1997).
28. Cowling, S. A. Plants and temperature: CO_2 uncoupling. *Science* **285,** 1500–1501 (1999).
29. McElwain, J. C. & Chaloner, W. C. The fossil cuticle as a skeletal record of environmental change. *Palaios* **11,** 376–388 (1996).
30. Retallack, G. J. *A Colour Guide to Paleosols* 117 (Wiley, Chichester, 1997).

Supplementary information is available on *Nature*'s World-Wide Web site (http://www.nature.com) or as paper copy from the London editorial office of *Nature*.

Acknowledgements

A. Liston provided herbarium specimens of *Ginkgo*, M. Shaffer helped with SEM imaging, and S. Tanaka supplied Japanese literature. W. Kürschner, D. Dilcher, S. Scheckler and V. Wilde offered useful botanical discussion. M. Manga and J. Wynn helped with curve fitting and diffusion equations.

Correspondence and requests for materials should be addressed to the author (e-mail: gregr@darkwing.uoregon.edu).

Strong coherence between solar variability and the monsoon in Oman between 9 and 6 kyr ago

U. Neff*, S. J. Burns†‡, A. Mangini*, M. Mudelsee§, D. Fleitmann† & A. Matter†

* *Heidelberg Academy of Sciences, Im Neuenheimer Feld 229, Heidelberg, Germany D-69120*
† *Geological Institute, University of Bern, Baltzerstrasse 1, Bern, Switzerland CH-3012*
§ *Institute of Meteorology, University of Leipzig, Stephanstrasse 3, Leipzig, Germany D-04103*

Variations in the amount of solar radiation reaching the Earth are thought to influence climate, but the extent of this influence on timescales of millennia to decades is unclear. A number of climate records show correlations between solar cycles and climate[1], but the absolute changes in solar intensity over the range of decades to millennia are small[2] and the influence of solar flux on climate is not well established. The formation of stalagmites in northern Oman has recorded past northward shifts of the intertropical convergence zone[3], whose northward migration stops near the southern shoreline of Arabia in the present climate[4]. Here we present a high-resolution record of oxygen isotope variations, for the period from 9.6 to 6.1 kyr before present, in a Th–U-dated stalagmite from Oman. The $\delta^{18}O$ record from the stalagmite, which serves as a proxy for variations in the tropical circulation and monsoon rainfall, allows us to make a direct comparison of the $\delta^{18}O$ record with the $\Delta^{14}C$ record from tree rings[5], which largely reflects changes in solar activity[6,7]. The excellent correlation between the two records suggests that one of the primary controls on centennial- to decadal-scale changes in tropical rainfall and monsoon intensity during this time are variations in solar radiation.

The Indian Ocean monsoon is one of the main weather systems on Earth, and variations in its intensity have broad oceanographic and economic effects. To date, studies of how and why the monsoon varies through time have been restricted to studies of meteorological records, which extend back about 150 years[8], or studies of lacustrine and marine sediments[9–12], which mainly yield information on millennial and longer timescales. At present, information on monsoon variation on decadal to centennial timescales is limited to identification of 'centennial-scale' changes in sedimentary records[13,14], but these studies lack the resolution to determine specific periodicities or forcing mechanisms. We have developed a high-resolution proxy for estimating variation in monsoon intensity by measuring past changes in $\delta^{18}O$ of monsoon rainfall as recorded in calcite $\delta^{18}O$ of a stalagmite.

Hoti cave is located in northern Oman on the southwestern side of the Oman mountains (57° 21′ E, 23° 05′ N, 800 m above sea level). The modern climate of the area is arid to semi-arid, and the area is not at present affected by the Indian Ocean monsoon system. However, numerous marine and continental palaeoclimate records indicate that the summer monsoon was considerably stronger during early to middle Holocene times than it is at present[9–12,15], accompanied by a shift in the northern limit of the monsoon rainfall belt far north of its modern location[15,16], which resulted in a continental pluvial period in the Sahel region of Africa, in Arabia and in India. In Hoti cave[3], the pluvial period led to deposition of a set of large stalagmites.

Here we present a high-resolution profile of $\delta^{18}O$ of stalagmite H5 from Hoti cave[3] on an improved timescale dated with 12 Th–U ages measured using mass spectrometry (see Methods for details). The speleothem covers the time span from 9.6 to 6.1 kyr before present (BP). It can be divided into four sections exhibiting different growth rates ranging from 0.03 to 0.57 mm yr^{-1} (Fig. 1). Samples (826) for stable isotope measurements were drilled from the core by hand with an average sampling interval of 0.4 mm, yielding an average time resolution for the core of 4.1 years. For the fastest growth interval (high-resolution interval), however, between 7.9 and 8.3 mm yr^{-1}, the resolution increases to 1.4 years.

The $\delta^{18}O$ values vary between −4‰ and −6‰ VPDB, reflecting the characteristically low $\delta^{18}O$ of monsoonal rainfall[17] (Fig. 2a). The values of the upper 4 mm, which are not displayed in Fig. 2a, increase to −1.5‰, marking the end of the Holocene pluvial period. Modern stalagmites in this cave also have comparatively positive $\delta^{18}O$ ranging from 0‰ to −2‰, corresponding to the present arid climate[3]. Measurements of $\delta^{18}O$ of modern cave waters and actively

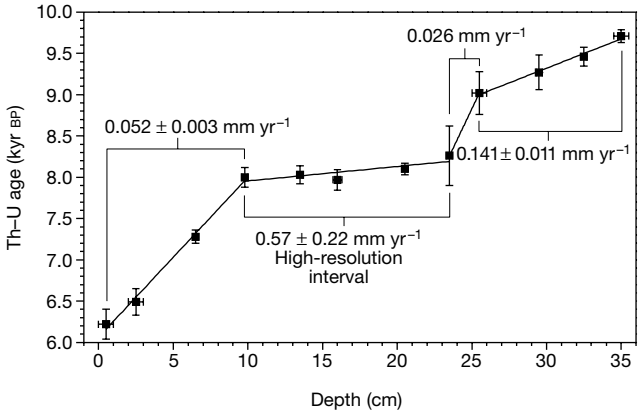

Figure 1 Plot of age versus depth for stalagmite H5. Twelve Th–U ages identify four sections with different growth rates varying between 0.03 and 0.57 mm yr^{-1}. All errors are 2σ (see Supplementary Information).

‡ Present address: Department of Geosciences, University of Massachusetts, Amherst, Massachusetts 01003, USA.

growing stalagmites show that calcite precipitation takes place in isotopic equilibrium[3], which was probably also the case for the wetter climate of early to middle Holocene times, when the relative humidity in the cave would have been greater. The variation of the $\delta^{18}O$ signal is very unlikely to be directly related to temperature changes because mean annual temperatures in the tropics have varied less than 1 °C during the Holocene[18], which could account for only 0.25‰ variation in calcite $\delta^{18}O$. Nor are the $\delta^{18}O$ values of precipitation in tropical areas correlated with temperature[17]. Kinetic effects on the $\delta^{18}O$ values[19] also seem unlikely because there is no observed relationship between H5 growth rates, which vary by a factor of 10, and its isotopic ratios. The $\delta^{18}O$ values of monsoonal rainfall and other types of rainfall associated with the ITCZ do, however, show an inverse correlation with rainfall amount[17,20]. We, therefore, ascribe the variation in $\delta^{18}O$ to changing rainfall intensity. Peaks of heavier $\delta^{18}O$ are associated with diminished monsoonal precipitation, due to either periodic southwards shifts of the ITCZ or periods of weaker monsoon, though it should be noted that the location of the ITCZ is not rigidly coupled to the variations of monsoon rainfall. As the $\delta^{18}O$ values of rainfall and ground water vary with changing intensity of monsoon rainfall, these variations are recorded in speleothem calcite.

The high temporal resolution of the speleothem $\delta^{18}O$ record enables a precise comparison with atmospheric $\Delta^{14}C$ measured in tree-rings[5] (Fig. 2a and b). This was done by further refining the Th–U timescale by tuning it to the $\Delta^{14}C$ timescale. We emphasize that the tuning was done while always remaining within the measurement error of each of the 12 Th–U ages along the profile, so that the net shift of any part of the $\delta^{18}O$ curve is only 190 years at most (Fig. 3). The similarity between the smoothed $\delta^{18}O$ and $\Delta^{14}C$ time series, both in their general patterns and in the number of peaks, is extremely strong. Even millennial-scale trends and relative amplitudes correspond. Furthermore, the high-resolution interval between 7.9 and 8.3 kyr BP also reveals a close correspondence between the two curves. The parallel evolution of $\delta^{18}O$ and $\Delta^{14}C$ seems very unlikely to have occurred by chance. Rather, the high correlation provides solid evidence that both signals are responding to the same forcing. Variations of $\Delta^{14}C$ were attributed to changes in the production rate in the stratosphere, induced by solar wind modulation of the cosmic ray flux. Maxima of ^{10}Be concentrations in polar ice cores that are synchronous with maxima in $\Delta^{14}C$ further reinforce this interpretation[6,7,21].

The high resolution and dating precision of the $\delta^{18}O$ record of H5 make it possible to perform a reliable frequency analysis. Spectral analyses of the untuned $\delta^{18}O$ record are given in Fig. 4a and b. The $\delta^{18}O$ results show statistically significant periodicities centred on 1,018, 226, 28, 10.7 and 9 years. Two broader sets of cycles are centred between 101–90 years and 35–26 years. These cycles are close to the periodicities of the tree-ring $\Delta^{14}C$ record (206, 148, 126, 89, 26 and 10.4 years), which are assigned to solar modulation[7]. Spectral analyses of $\delta^{18}O$ values of foraminifera from sediments in the South China Sea also suggest monsoon cycles of around 1,000 (775) and 100–90 years (ref. 22).

We performed an additional spectral analysis of the tuned $\delta^{18}O$ record (Fig. 4c and d). The shape of the tuned spectra is rather similar to that of the untuned spectra. The tuned time series is somewhat shorter than the untuned one. Therefore all peaks of the tuned spectra are moved to somewhat shorter periods. Owing to the tuning, the noise between the significant peaks decreases. Statistically significant periodicities are centred on 779, 205, 134 and 87 years. The latter cycle is particularly strengthened in the tuned spectral analysis, as the two separate cycles at 101 and 90 years are joined in one stronger peak. The broad set of peaks around 28–23 years is present in both analyses as well as the two peaks at 10 and 9 years. Spectral analysis of the tuned high-resolution interval reveals further cycles with periodicities of 24, 7.5 and 3 years. Perhaps not surprisingly, the tuned timescale results in a cycle pattern that even more closely matches the periodicities of $\Delta^{14}C$ (206, 148, 126, 89, 26 and 10.4 years)[7]. The cross-spectral analysis (Fig. 5) of these two time series further confirms the correspondence

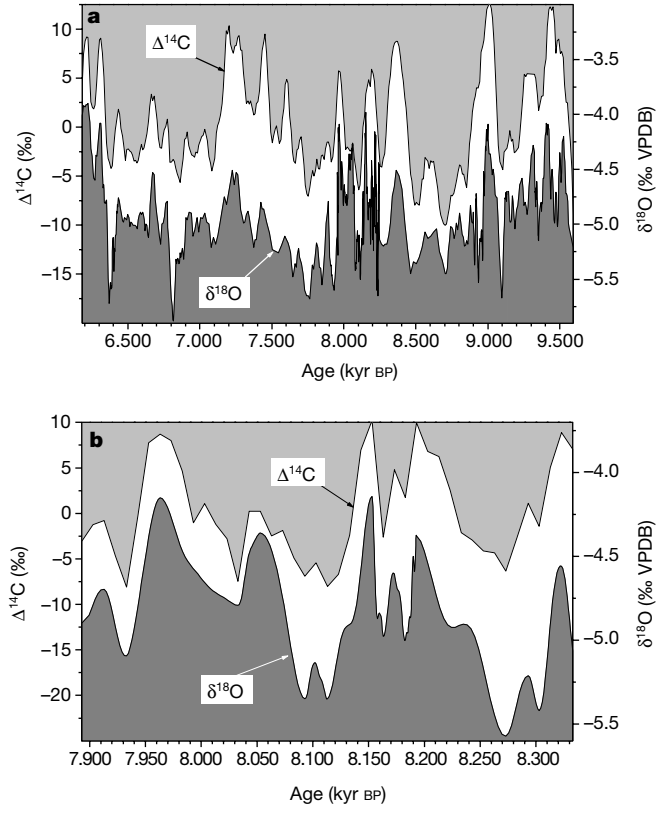

Figure 2 Profiles of H5 $\delta^{18}O$ values and atmospheric $\Delta^{14}C$. **a**, The entire H5 record (826 samples); **b**, the high-resolution interval. Both profiles in **a** were smoothed with 5-point adjacent averaging for better visual comparison. The $\delta^{18}O$ profile in **b** was filtered with 7-point fast Fourier transform smoothing (cut-off frequency, 0.1 yr^{-1}). The correlation coefficient of the unsmoothed data is $r = 0.60$, $P(>|r|) < 10^{-8}$ in **a**, and $r = 0.55$, $P(>|r|) = 1.1\times10^{-4}$ in **b**. Because of the apparent good relationship between the two profiles, we fine-tuned the peaks of the $\delta^{18}O$ age profile to the peaks of the $\Delta^{14}C$ record. The corrections of the Th–U timescale are shown in Fig. 3.

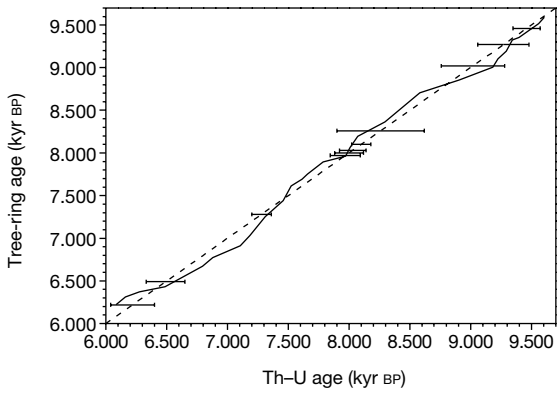

Figure 3 Measured (dashed line) and optimized (solid line) Th–U age scales for stalagmite H5. The error bars are the uncertainties of the Th–U ages. The correlation between the time series of $\delta^{18}O$ and $\Delta^{14}C$ was made using the adjusted Th–U timescale. As shown, the optimized timescale always remains within the uncertainty of the individual Th–U dates, both for the entire profile of $\delta^{18}O$ and for the high-resolution interval.

of the periodicities. This similarity suggests a solar forcing of the Hoti cave palaeoprecipitation record, and by extension, of the Indian Ocean monsoon, during this period.

The periodicities in the high-resolution interval are similar to the cycles of 24, 7.5 and 3.2 years that have been noted for the North Atlantic Oscillation[23], suggesting that at these shorter timescales the North Atlantic climate system might also be a cause of changes in the amount of monsoon rainfall in the Hoti cave area. In particular, it has been suggested that the 512-year cycle in $\Delta^{14}C$, which is within the bandwidth around the 779-year cycle in the H5 record, is caused by variations in ocean circulation[7]—specifically, by changes in North Atlantic Deep Water (NADW) formation that control incorporation of ^{14}C into the ocean[24]. Periods of decreased NADW formation (decreased surface heat flux to the North Atlantic Ocean) should be associated with longer, colder Eurasian winters, leading to increased snow cover on the Tibetan plateau and a delayed or and weakened monsoon the following summer[25,26].

In summary, the $\delta^{18}O$ record of the stalagmite H5 from Hoti cave represents a precisely dated high-resolution time series of the intensity of Indian Ocean monsoonal rainfall. The strong similarity between the smoothed secular variation curves of the H5 $\delta^{18}O$ isotopic record and the $\Delta^{14}C$ record—together with their spectral analyses—suggest that both are responding to the same climate forcing. Much of the variation in $\Delta^{14}C$ is attributed to solar forcing through variations in solar activity and intensity[7]. Thus, to the extent that centennial and decadal variations in the $\Delta^{14}C$ record are controlled by changes in global solar radiation, so should such changes control the intensity of the Indian Ocean monsoon. Less clear is the mechanism by which solar variability affects the monsoon. The variations in solar irradiance necessary to cause the observed changes in $\Delta^{14}C$ are probably of the order of a few tenths of one per cent (ref. 2). Such minor variations are unlikely to have directly caused significant differences in sensible heating of the Tibetan plateau. It is more likely that solar variability leads to changes in atmospheric or oceanic circulation that amplify this initial input. For example, a model study of the relationship between the 11-year solar cycle and climate has suggested that maximum solar irradiance leads to increased easterly trade winds and a broadened Hadley cell[27]. □

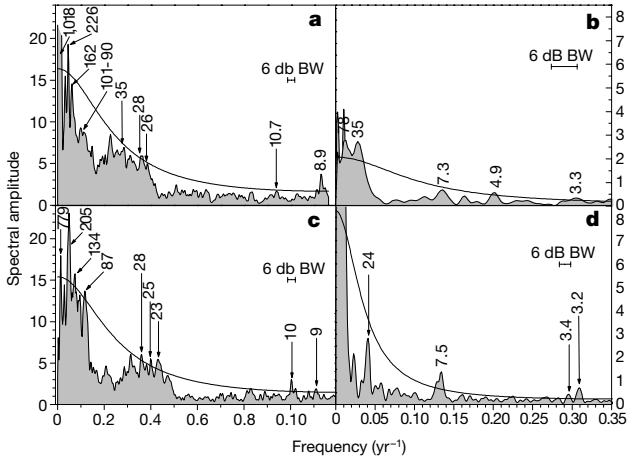

Figure 4 Frequency analysis of the H5 $\delta^{18}O$ record for the entire sample and for the high-resolution interval. **a**, **b**, Untuned; **c**, **d**, tuned. Peaks are labelled with their period (in years). Spectral power was estimated with the SPECTRUM package[30], which uses the Lomb–Scargle periodogram for unevenly spaced data. The number (n_{seg}) of overlapping (50%) segments is 6 (**a** and **c**) and 3 (**b** and **d**). The spectral window is a Welch I type. The 6-dB bandwidth (BW) determines the frequency resolution. Smooth line, red-noise background (upper 90% χ^2 bound).

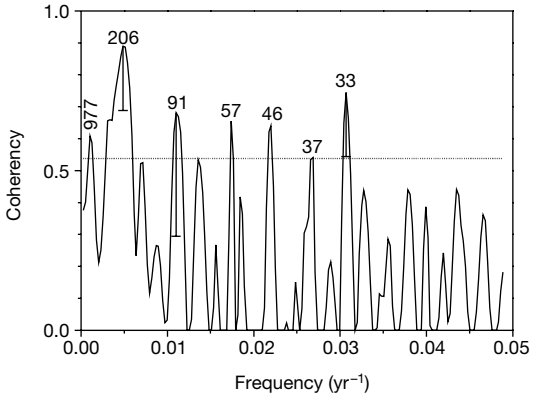

Figure 5 Cross-spectral analysis[30] of the tuned H5 $\delta^{18}O$ record for the entire studied sample versus the $\Delta^{14}C$ record (ref. 4). The same spectral parameters (n_{seg} = 6, Welch I window) as for the univariate (Fig. 4c) analysis were used. Peaks common to both time series are labelled with their period (in years). Error bars are given as lower 95% bounds. Horizontal line is 5% false-alarm level[30].

Methods

Th–U ages

Analytical procedures for the separation and purification of Th and U were as described in ref. 28. Th–U measurements were performed on a multicollector mass spectrometer (Finnigan MAT 262 RPQ) with a double filament technique. Thorium and uranium were measured in peak-jump mode and semi-peak-jump mode, respectively. Calibration of Faraday cup to ionization efficiency was made adopting the natural $^{238}U/^{235}U$ of 137.88. To determine the uranium and thorium concentrations, defined quantities of a $^{233}U/^{236}U$ double spike and a ^{229}Th spike were added. Th–U ages were corrected for detritus following ref. 29 assuming a $^{232}Th/^{238}U$ isotope ratio of 3.8. The reproducibility of the isotope ratio of $^{234}U/^{238}U$ and the concentration of ^{232}Th of standard materials is 0.3% and 0.8% (2σ), respectively. For details about measurements of standard material, see ref. 29.

Oxygen isotopes

Oxygen isotope ratios are expressed in δ-notation, the per mil deviation from the VPDB standard: $\delta^{18}O = [((^{18}O/^{16}O)_{sample}/(^{18}O/^{16}O)_{VPDB}) - 1] \times 1{,}000$. For each measurement, approximately 3 mg of powder was drilled from the sample and analysed with an on-line, automated, carbonate preparation system linked to a VG Prism ratio mass spectrometer. Reproducibility of standard materials is 0.08‰ for $\delta^{18}O$.

Received 14 September 2000; accepted 26 March 2001.

1. Hoyt, D. V. & Schatten, K. H. *The Role of the Sun in Climate Change* (Oxford Univ. Press, New York, 1997).
2. Fligge, M. & Solanki, S. K. The solar spectral irradiance since 1700. *Geophys. Res. Lett.* **26,** 2465–2468 (1999).
3. Burns, S. J., Matter, A., Frank, N. & Mangini, A. Speleothem-based paleoclimate record from northern Oman. *Geology* **26,** 499–502 (1998).
4. Hastenrath, S. *Climate and Circulation of the Tropics* (Reidel, Boston, 1985).
5. Stuiver, M. *et al.* INTCAL98 Radiocarbon age calibration, 24,000–0 cal BP. *Radiocarbon* **40,** 1041–1083 (1998).
6. Beer, J., Mende, W. & Stellmacher, R. The role of the sun in climate forcing. *Quat. Sci. Rev.* **19,** 403–415 (2000).
7. Stuiver, M. & Braziunas, T. F. Sun, ocean climate and atmospheric $^{14}CO_2$: an evaluation of causal and spectral relationships. *Holocene* **3,** 289–305 (1993).
8. Sontakke, N. A., Plant, G. B. & Singh, N. Construction of all-India summer monsoon rainfall series for the period 1844-1991. *J. Clim.* **6,** 1807–1811 (1993).
9. Clemens, S. C., Murray, D. W. & Prell, W. L. Nonstationary phase of the Plio-Pleistocene Asian monsoon. *Science* **274,** 943–948 (1996).
10. Overpeck, J., Anderson, D., Trumbore, S. & Prell, W. The southwest Indian Monsoon over the last 18 000 years. *Clim. Dyn.* **12,** 213–225 (1996).
11. Bryson, R. A. & Swain, A. M. Holocene variations of monsoon rainfall in Rajasthan. *Quat. Res.* **16,** 135–145 (1981).
12. Gasse, F., Tehet, R., Durand, A., Gibert, E. & Fontes, J.-C. The arid-humid transition in the Sahara and the Sahel during the last deglaciation. *Nature* **346,** 141–146 (1990).
13. Lamb, H. F. *et al.* Relation between century-scale Holocene arid intervals in tropical and temperate zones. *Nature* **373,** 134–137 (1995).
14. Sirocko, F. *et al.* Century-scale events in monsoonal climate over the last 24,000 years. *Nature* **364,** 322–324 (1993).
15. Liu, K., Yao, Z. & Thompson, L. G. A pollen record of Holocene climatic changes from the Dunde ice cap, Qinghai-Tibetan Plateau. *Geology* **26,** 135–138 (1998).
16. Ritchie, J. C., Eyles, C. H. & Haynes, C. V. Sediment and pollen evidence for an early to mid-Holocene humid period in the eastern Sahara. *Nature* **314,** 352–355 (1985).

17. Rozanski, K., Araguás-Araguás, L. & Gonfiantini R. in *Climate Change in Continental Isotopic Records* (eds Swart, P. K., Lohmann, K. C., McKenzie, J. & Savin, S.) 1–36 (American Geophysical Union Geophysical Monograph 78, Washington DC, 1993).
18. COHMAP Members. Climatic changes of the last 18 000 years: observations and model simulations. *Science* **241,** 1043–1052 (1988).
19. Hendy, C. H. The isotopic geochemistry of speleothems - I. The calculation of the effects of different modes of formation on the isotopic composition of speleothems and their applicability as paleoclimate indicators. *Geochim. Cosmochim. Acta.* **35,** 801–824 (1971).
20. Technical Report Series No. 331, 781 (International Atomic Energy Agency, Vienna, 1992).
21. Lean, J., Beer, J. & Bradley, R. Reconstruction of solar irradiance since 1610: Implications for climate change. *Geophys. Res. Lett.* **22,** 3195–3198 (1995).
22. Wang, L. *et al.* East Asian monsoon climate during the Late Pleistocene: high resolution sediment records from the South China Sea. *Mar. Geol.* **156,** 245-284 (1999).
23. Cook, E. R., D'Arrigo, R. D. & Briffa, K. R. A reconstruction of the North Atlantic oscillation using tree-ring chronologies from North America and Europe. *Holocene* **8,** 9–17 (1998).
24. Stocker, T. F. & Wright, D. G. Rapid changes in ocean circulation and atmospheric radiocarbon. *Paleoceanography* **11,** 773–795 (1996).
25. Dickson, R. R. Eurasian snow cover versus Indian monsoon rainfall—An extension of the Hahn-Shukla results. *J. Clim. Appl. Meteorol.* **23,** 171–173 (1984).
26. Meehl, G. A. Influence of the land surface in the Asian summer monsoon, external conditions versus internal feedbacks. *J. Clim.* **7,** 1033–1049 (1994).
27. Haigh, J. D. The impact of solar variability on climate. *Science* **272,** 981–984 (1996).
28. Ivanovich, M. & Harmon, R. S. *Uranium Series Disequilibrium: Applications to Environmental Problems* (Clarendon, Oxford, 1993).
29. Frank, N., Braun, M., Hambach, U., Mangini, A. & Wagner, G. Warm period growth of travertine during the last interglaciation in southern Germany. *Quat. Res.* **54,** 38–48 (2000).
30. Schulz, M. & Stattegger, K. Spectral analysis of unevenly spaced paleoclimatic time series. *Comput. Geosci.* **23,** 929–945 (1997).

Supplementary information is available on *Nature*'s World-Wide Web site (http://www.nature.com) or as paper copy from the London editorial office of *Nature*.

Acknowledgements

We thank D. Sanz for caving assistance; R. Eichstädter for technical assistance; M. Stuiver, A. Baker and D. Ford for suggestions; and S. Clemens for comments.

Correspondence and requests for materials should be addressed to S.B. (e-mail: sburns@geo.umass.edu).

Metamorphic devolatilization of subducted marine sediments and the transport of volatiles into the Earth's mantle

D. M. Kerrick* & J. A. D. Connolly†

* *Department of Geosciences, The Pennsylvania State University, University Park, Pennsylvania 16802, USA*
† *Earth Sciences Department, Swiss Federal Institute of Technology, 8092 Zurich, Switzerland*

Volatiles, most notably CO_2, are recycled back into the Earth's interior at subduction zones[1,2]. The amount of CO_2 emitted from arc volcanism appears to be less than that subducted, which implies that a significant amount of CO_2 either is released before reaching the depth at which arc magmas are generated or is subducted to deeper depths. Few high-pressure experimental studies[3–5] have addressed this problem and therefore metamorphic decarbonation in subduction zones remains largely unquantified, despite its importance to arc magmatism, palaeoatmospheric CO_2 concentrations and the global carbon cycle[6]. Here we present computed phase equilibria to quantify the evolution of CO_2 and H_2O through the subduction-zone metamorphism of carbonate-bearing marine sediments (which are considered to be a major source for CO_2 released by arc volcanoes[6]). Our analysis indicates that siliceous limestones undergo negligible devolatilization under subduction-zone conditions. Along high-temperature geotherms clay-rich marls completely devolatilize before reaching the depths at which arc magmatism is generated, but along low-temperature geotherms, they undergo virtually no devolatilization. And from 80 to 180 km depth, little devolatilization occurs for all carbonate-bearing marine sediments. Infiltration of H_2O-rich fluids therefore seems essential to promote subarc decarbonation of most marine sediments. In the absence of such infiltration, volatiles retained within marine sediments may explain the apparent discrepancy between subducted and volcanic volatile fluxes and represent a mechanism for return of carbon to the Earth's mantle.

A premise of our work is that realistic modelling of metamorphic devolatilization of subducted lithologies is only possible on the basis of phase equilibria in chemical systems closely approximating actual bulk compositions. Our studies on metamorphic devolatilization of the other two main carbonate-bearing lithologies involved in subuction zones (ophicarbonates and metabasalts) are considered elsewhere[2,7]. Carbonate is abundant in two main pelagic marine sediment lithologies[8]: (1) siliceous limestones and (2) clay-carbonates (marls). From the database of ref. 8 (see Supplementary Information) we selected bulk compositions of siliceous limestones from the Marianas and Vanuatu trenches, a marl from the Antilles trench and their average marine sediment bulk composition (denoted 'GLOSS' in ref. 8). Our computations account for the oxide components: SiO_2, Al_2O_3, FeO, MgO, CaO, Na_2O, K_2O, CO_2 and H_2O.

For each marine sediment bulk composition, the corresponding phase diagram section (Fig. 1) was computed as a function of pressure (P) and temperature (T) by free-energy minimization[9]. The thermodynamic database of ref. 10 was used for the properties of all end-member species, and mineral solutions were modelled as described elsewhere[9]. Thermodynamic data for H_2O, CO_2 and their mixtures were computed from the equation of state given in ref. 11. To track metamorphic devolatilization along the top of subducted slabs, we adopted the geotherms[12] for the subduction zones of northwestern and southeastern Japan (Fig. 1). These geotherms are reasonable approximations for the respective extremal low-temperature and high-temperature geotherms for subduction zones (S. M. Peacock, personal communication).

Because of compositional degrees of freedom in the crystalline and fluid phases, the phase diagram sections are dominated by multivariant phase fields. Consequently, both mineral modes and compositions vary continuously along geotherms (Fig. 2). Phase relations along geotherms up to a pressure $P \approx 3$ GPa change significantly (Fig. 1) because of intersection with numerous phase field boundaries. However, at $P > 3$ GPa, the geotherms are subparallel to the phase field boundaries (Fig. 1); consequently, little reaction occurs along geotherms at $P > 3$ GPa. The differences between these regimes are illustrated in Fig. 2. Accordingly, significant changes in the mineralogy and mineral proportions occur up to ~800 °C ($P \approx 3$ GPa) whereas there is comparatively little variation above ~800 °C.

The fluid composition (Fig. 2) is controlled by multivariant equilibria involving carbonates and hydrous phases. The rise in the mole fraction of CO_2, X_{CO_2}, up to ~750 °C correlates with consumption of carbonates (Fig. 2), whereas the diminution in X_{CO_2} above ~750 °C occurs because of aragonite production. To track loss of volatiles we computed the percentage (by weight; wt%) of H_2O and CO_2 for carbonate-bearing marine sediments as a function of pressure and temperature (Fig. 3). In the lower-pressure half of Fig. 3, the negative P–T slopes of the wt% H_2O isopleths reflect negative slopes of phase field boundaries (Fig. 1). In contrast to isopleths with negative slopes at lower pressures, isopleths are subparallel to geotherms at $P > 2$–3 GPa (Fig. 3).

Siliceous limestones release about 1 wt% CO_2 and 1 wt% H_2O along the high-temperature geotherm (Fig. 3c, d). Because less CO_2